Clinical Molecular Imaging of Chemokine Receptor CXCR4 Expression in Atherosclerotic Plaque Using ^{68}Ga-Pentixafor PET: Correlation with Cardiovascular Risk Factors and Calcified Plaque Burden

Desiree Weiberg[1], James T. Thackeray[1], Guenter Daum[2], Jan M. Sohns[1], Saskia Kropf[3], Hans-Juergen Wester[4], Tobias L. Ross[1], Frank M. Bengel[1], and Thorsten Derlin[1]

[1]Department of Nuclear Medicine, Hannover Medical School, Hannover, Germany; [2]Department of Vascular Medicine, University Heart Center Hamburg-Eppendorf, Hamburg, Germany; [3]Scintomics GmbH, Fürstenfeldbruck, Germany; and [4]Pharmaceutical Radiochemistry, Technical University of Munich, Munich, Germany

The CXC-motif chemokine receptor 4 (CXCR4) represents a promising target for molecular imaging of different CXCR4-positive cell types in cardiovascular diseases such as atherosclerosis and arterial wall injury. The aim of this study was to assess the prevalence, pattern, and clinical correlates of arterial wall accumulation of ^{68}Ga-pentixafor, a specific CXCR4 ligand for PET. **Methods:** The data for 51 patients who underwent ^{68}Ga-pentixafor PET/CT for noncardiovascular indications were retrospectively analyzed. Tracer accumulation in the vessel wall of major arteries was analyzed qualitatively and semiquantitatively by blood-pool–corrected target-to-background ratios. Tracer uptake was compared with calcified plaque burden and cardiovascular risk factors. **Results:** Focal arterial uptake of ^{68}Ga-pentixafor was seen at 1,411 sites in 51 (100%) of patients. ^{68}Ga-pentixafor uptake was significantly associated with calcified plaque burden ($P < 0.0001$) and cardiovascular risk factors including age ($P < 0.0001$), arterial hypertension ($P < 0.0001$), hypercholesterolemia ($P = 0.0005$), history of smoking ($P = 0.01$), and prior cardiovascular events ($P = 0.0004$). Both the prevalence ($P < 0.0001$) and the signal intensity ($P = 0.009$) of ^{68}Ga-pentixafor uptake increased as the number of risk factors increased. **Conclusion:** ^{68}Ga-pentixafor PET/CT is suitable for noninvasive, highly specific PET imaging of CXCR4 expression in the atherosclerotic arterial wall. Arterial wall ^{68}Ga-pentixafor uptake is significantly associated with surrogate markers of atherosclerosis and is linked to the presence of cardiovascular risk factors. ^{68}Ga-pentixafor signal is higher in patients with a high-risk profile and may hold promise for identification of vulnerable plaque.

Key Words: CXCR4; atherosclerosis; plaque; ^{68}Ga-pentixafor; PET/CT

J Nucl Med 2018; 59:266–272
DOI: 10.2967/jnumed.117.196485

The CXC-motif chemokine receptor 4 (CXCR4) and its ligand, CXCL12, play an important role in trafficking of progenitor and inflammatory cells (*1*). Ex vivo data have demonstrated a progressive accumulation of CXCR4-positive cells during plaque evolution (*1*). The role of the CXCR4/CXCL12 axis has recently been emphasized in models of ischemic injury (*2–6*). Of note, vulnerable plaque is characterized by distinct histopathologic hallmarks, including a preponderance of inflammatory CXCR4-positive cells such as monocytes and macrophages (*1,7*). Furthermore, CXCR4 is also expressed by other leukocyte populations and, importantly, various cell types such as smooth muscle cell progenitors and endothelial progenitor cells contributing to plaque evolution (*1*). Therefore, we hypothesized that CXCR4 would be a suitable target for imaging of plaque pathophysiology.

PET has become a well-studied technique for noninvasive molecular imaging of various aspects of atherosclerosis (*8*), such as for the quantification of macrophage-mediated inflammation in atherosclerotic lesions using ^{18}F-FDG (*9,10*). However, ^{18}F-FDG exhibits several inherent limitations, including a nonspecific mechanism of uptake, physiologic uptake in brain and myocardium, interaction with blood glucose, and the requirement for a fasting period before imaging.

Recently, the highly specific radiotracer ^{68}Ga-pentixafor was introduced for clinical molecular imaging of CXCR4 expression (*11–14*). Our group reported on the feasibility of ^{68}Ga-pentixafor PET for noninvasive characterization of postinfarction myocardial inflammation. In mice after coronary artery ligation, CXCR4 upregulation was proportional to flow cytometry–derived elevation of CD45-positive leukocytes in the left ventricle and increased immunohistochemical detection of CD68-positive macrophages and Ly6G-positive granulocytes in the infarct territory (*5*). More recently, ^{68}Ga-pentixafor PET detected CXCR4 expression by inflammatory cells present in atherosclerotic plaques of an experimental rabbit model and in a limited patient cohort (*15*). The immunohistochemistry of human carotid plaques demonstrated CXCR4 expression localized to regions with high CD68-positive macrophage content (*15*).

However, experience with and interpretation of ^{68}Ga-pentixafor PET imaging of arterial wall physiology in humans remain limited. Therefore, the purpose of the present study was to assess the

Received May 23, 2017; revision accepted Jul. 7, 2017.
For correspondence or reprints contact: Thorsten Derlin, Department of Nuclear Medicine, Hannover Medical School, Carl-Neuberg-Strasse 1, D-30625 Hannover, Germany.
E-mail: derlin.thorsten@mh-hannover.de
Published online Aug. 3, 2017.

prevalence, distribution, and topographic relationship of arterial lesions with increased ^{68}Ga-pentixafor accumulation as determined by PET relative to arterial calcification as determined by CT.

MATERIALS AND METHODS

Study Population

The population of this retrospective study consisted of 51 patients (12 women, 39 men; mean age ± SD, 59.5 ± 16.2 y; range, 22.7–85.0 y) who had been referred to our institution for a ^{68}Ga-pentixafor PET/CT scan for various noncardiovascular clinical indications (interstitial lung disease, $n = 21$; sarcoidosis, $n = 13$; complicated urinary tract infection, $n = 8$; leukemia, $n = 5$; and miscellaneous, $n = 4$) between February 2015 and June 2016. Sex, age (at-risk age: women, >55 y; men, >45 y), and other common cardiovascular risk factors such as hypertension, hypercholesterolemia, diabetes, a smoking habit, and prior vascular events (defined as myocardial infarction or cerebrovascular insult) were documented for each patient (*16*). Risk factors were considered categoric variables. Because of the potential influence of statins on plaque physiology and on expression of CXCR4 on monocytes, treatment with statins was also recorded (*17*). The exclusion criteria were a history of vasculitis, chemotherapy in the preceding 4 wk, or a cardiovascular event in the preceding 6 mo. The protocol complied with the Declaration of Helsinki. The institutional review board approved this retrospective study, and the requirement to obtain informed consent was waived.

Radiolabeling of ^{68}Ga-Pentixafor, Image Acquisition, and Reconstruction

Material for synthesis of ^{68}Ga-pentixafor (CPCR4.2) was provided by Scintomics. Synthesis was performed using a cold mass of 15 nmol of CPCR4.2 and a 1.11-GBq ^{68}Ge/^{68}Ga-generator (Eckert and Ziegler) connected to a Scintomics good-radiopharmaceutical-practice synthesis module, as described previously (*12–14,18*).

All studies were obtained on a dedicated PET/CT system (Biograph mCT 128 Flow; Siemens) equipped with an extended-field-of-view PET component, a 128-slice spiral CT component, and a magnetically driven table optimized for continuous scanning. ^{68}Ga-pentixafor was injected intravenously at a dose of 123 ± 32 MBq. After an uptake period of 60 min, imaging started with a single low-dose nonenhanced helical CT scan (120 kV, modulated amperage, pitch of 1.2, and reconstructed axial slice thickness of 5.0 mm) obtained for attenuation correction of the PET acquisitions. Whole-body PET images were acquired using continuous bed motion at a speed of 2.0 mm/s for the head, 0.5 mm/s for the chest and abdomen, and 2.5 mm/s for the legs. All studies were reconstructed using time-of-flight and point-spread function TrueX information combined with an iterative algorithm (Ultra HD; Siemens Healthcare [2 iterations, 21 subsets, matrix of 200, zoom of 1.0, and gaussian filter of 2.0]).

Image Analysis

Transaxial PET, CT, and fused PET/CT ^{68}Ga-pentixafor images were analyzed both visually and semiquantitatively on a dedicated workstation (syngo.via, V10B; Siemens Healthcare). The scans were analyzed on the basis of patients, arterial segment, and lesions. For segment-based analysis, the major arteries were subdivided as follows: right and left common carotid arteries, thoracic aorta, abdominal aorta, right and left iliac arteries, and right and left femoral arteries.

Calcified Plaque (CP). CPs were defined as high-density mural areas (attenuation > 130 Hounsfield units) in the wall of the studied arteries (*19*). First, CT images were visually analyzed for the presence of CPs. Patients were categorized as those with CP (CT-positive) and those without discernible CP (CT-negative). The calcified lesion thickness, defined as the maximum calcification diameter measured in the intimoadventitial direction, was measured. Each arterial segment was classified on a 5-point scale for grading the maximum circumferential extent of calcifications: 0, absent; 1, less than 25% of arterial wall circumference; 2, 25%–50% of arterial wall circumference; 3, 51%–75% of arterial wall circumference; and 4, greater than 75% of arterial wall circumference (*16*).

Radiotracer Uptake. PET images were visually evaluated for the presence of focal radiotracer uptake above the background level in arterial walls (PET-positive). The localization of PET-positive lesions in relation to CPs and the vascular wall was analyzed on PET/CT images. Semiquantitative analysis was performed by obtaining the

TABLE 1
Characteristics of Study Population ($n = 51$)

Characteristic	CT-positive	PET-positive	PET-positive/CT-positive	PET-positive/CT-negative	Total population
Subjects	42 (82.4)	51 (100)	42 (82.4)	9 (17.6)	51 (100)
Age (y)					
Mean ± SD	64.9 ± 11.8	59.5 ± 16.2	64.9 ± 11.8	34.6 ± 8.8	59.5 ± 16.2
Range	26.8–85.0	22.7–85.0	26.8–85.0	22.7–50.4	22.7–85.0
Of at-risk age	31 (73.8)	39 (76.5)	31 (73.8)	8 (88.9)	39 (76.5)
Male sex	32 (76.2)	39 (76.5)	32 (76.2)	7 (77.8)	39 (76.5)
Cardiovascular risk factors					
Hypertension	29 (69.0)	32 (62.7)	29 (69.0)	3 (33.0)	32 (62.7)
Hypercholesterolemia	21 (50.0)	22 (43.1)	21 (50.0)	1 (11.0)	22 (43.1)
Diabetes mellitus	9 (21.4)	10 (19.6)	9 (21.4)	1 (11.0)	10 (19.6)
History of smoking	33 (78.6)	38 (74.5)	33 (78.6)	5 (55.6)	38 (74.5)
Prior vascular event	11 (26.2)	11 (21.6)	11 (26.2)	0 (0.0)	11 (21.6)
Statin medication	16 (38.1)	17 (33.3)	16 (38.1)	1 (11.0)	17 (33.3)

Qualitative data are expressed as numbers followed by percentages in parentheses; continuous data are expressed as mean ± SD.

TABLE 2
Prevalence, Distribution, and Intensity of ^{68}Ga-Pentixafor Uptake

Characteristic	Common carotid artery		Thoracic aorta	Abdominal aorta	Iliac artery		Femoral artery		Total
	Right	Left			Right	Left	Right	Left	
Patients with uptake in artery wall	30 (58.8)	27 (52.9)	50 (98.0)	50 (98.0)	43 (84.3)	42 (82.4)	44 (86.3)	44 (86.3)	51 (100.0)
Uptake sites	49 (3.5)	55 (3.9)	339 (24.0)	369 (26.2)	115 (8.2)	115 (8.2)	180 (12.8)	189 (13.4)	1,411 (100.0)
Colocalization with calcification	14 (28.6)	15 (27.3)	43 (12.7)	156 (42.3)	49 (42.6)	53 (46.1)	70 (38.9)	73 (38.6)	473 (33.5)
SUV_{max}									
Mean ± SD	2.9 ± 0.5	2.9 ± 0.5	3.3 ± 0.6	3.6 ± 0.8	3.4 ± 0.7	3.4 ± 0.6	3.3 ± 0.6	3.4 ± 0.7	3.4 ± 0.7
Range	2.2–4.5	2.3–4.9	2.0–6.1	1.8–7.3	2.4–5.3	2.0–5.3	2.0–5.4	1.9–6.6	1.8–7.3
TBR									
Mean ± SD	1.7 ± 0.4	1.6 ± 0.4	1.9 ± 0.4	2.1 ± 0.6	1.9 ± 0.4	2.0 ± 0.5	1.9 ± 0.5	2.1 ± 0.6	2.0 ± 0.5
Range	1.1–2.8	1.1–2.9	1.2–4.3	1.2–4.9	1.2–3.1	1.2–3.9	1.2–4.3	1.2–4.4	1.1–4.9

Data are numbers followed by percentages in parentheses, unless otherwise indicated.

SUV_{max} of a lesion through manually placing an individual 3-dimensional volume of interest (typically 10 mm in diameter) around the lesion on coregistered transaxial PET/CT images. $SUV_{blood\ pool}$ was measured as the mean from 3 regions of interest of fixed size (10 mm) placed in the mid lumen of the superior vena cava. For the calculation of the arterial target-to-background ratio (TBR), the SUV of each arterial lesion was divided by the $SUV_{blood\ pool}$ (*10*).

Statistical Analysis

Continuous variables are expressed as mean ± SD. Categoric variables are presented with absolute and relative frequencies. For between-group comparisons of parametric continuous data, *P* values were calculated from an unpaired Student *t* test. The Pearson correlation coefficient (*r*) was used to assess the relationship between PET and CT findings, as well as imaging findings and cardiovascular risk factors. Afterward, a stepwise multiple-regression analysis was performed to determine an independent association between the imaging findings (number of CPs, number of PET-positive foci, and TBR) and cardiovascular risk factors. TBR divided into quartiles was analyzed using 1-way ANOVA. Statistical significance was established for *P* values of less than 0.05. Statistical analysis was performed using Prism (version 6.0 for Mac OS X [Apple]; GraphPad Software Inc.) and MedCalc Statistical Software (version 17.1; MedCalc Software).

RESULTS

^{68}Ga-pentixafor uptake measurements and the assessment of CP burden were feasible in all patients. Relevant clinical patient characteristics are reported in Table 1.

TABLE 3
Prevalence, Distribution, and Extent of Calcification

Characteristic	Common carotid artery		Thoracic aorta	Abdominal aorta	Iliac artery		Femoral artery		Total
	Right	Left			Right	Left	Right	Left	
Patients with calcification sites	25 (49.0)	23 (45.1)	36 (70.6)	40 (78.4)	39 (76.5)	35 (68.6)	35 (68.6)	35 (68.6)	42 (82.4)
Calcification sites	175 (2.7)	135 (2.1)	891 (13.8)	1,735 (26.9)	706 (10.9)	615 (9.5)	1,119 (17.3)	1,080 (16.7)	6,456 (100)
Sites per affected segment									
Mean ± SD	7.0 ± 5.2	5.9 ± 4.0	24.8 ± 23.5	43.4 ± 33.8	18.1 ± 14.6	17.6 ± 13.4	32.0 ± 29.5	30.9 ± 28.4	24.1 ± 25.4
Range	1–24	2–18	1–86	1–125	1–59	2–48	1–122	1–110	1–125
Calcification score (mean ± SD)	2.2 ± 1.1	1.7 ± 0.9	1.3 ± 0.6	2.9 ± 1.3	1.9 ± 1.0	2.1 ± 1.1	2.5 ± 1.2	2.4 ± 1.2	2.1 ± 1.1
Lesion thickness (mm)									
Mean ± SD	2.4 ± 0.8	2.3 ± 1.0	3.1 ± 1.2	3.9 ± 1.7	3.1 ± 1.0	3.1 ± 1.0	2.1 ± 0.8	2.0 ± 0.9	2.8 ± 1.3
Range	1–4	1–4	1–5	1–8	1–5	1–5	1–4	1–5	1–8

Data are numbers followed by percentages in parentheses, unless otherwise indicated.

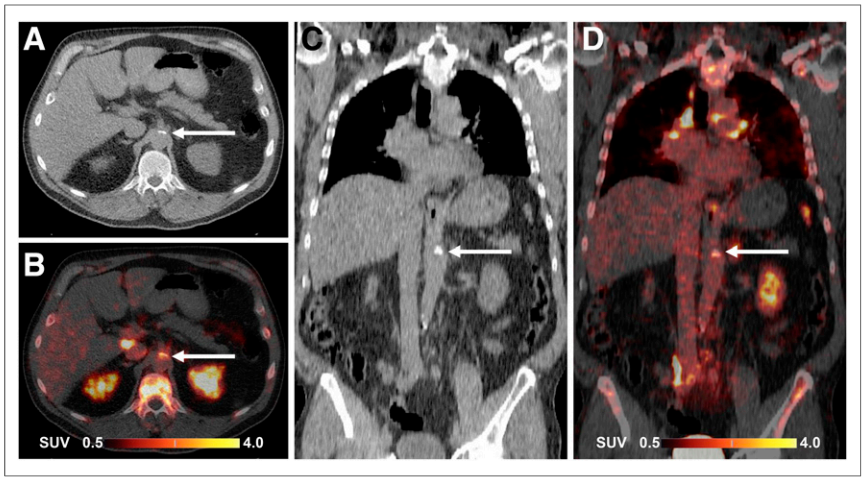

FIGURE 1. ^{68}Ga-pentixafor PET/CT images of abdominal aorta in 64-y-old man. CT (A and C) and PET/CT (B and D) images in transaxial (A and B) and coronal (C and D) views show ^{68}Ga-pentixafor uptake in calcified atherosclerotic lesion (arrows) coincident with calcification.

Arterial Wall ^{68}Ga-Pentixafor Uptake and CP Burden

Focally increased ^{68}Ga-pentixafor uptake in the arterial wall (Table 2) was observed at 1,411 sites in 51 (100%) patients. The prevalence of uptake was the highest in the abdominal aorta, followed by the thoracic aorta. Mean SUV_{max} was 3.4 ± 0.7, with a range of 1.8–7.3. Mean $SUV_{blood\ pool}$ was 1.8 ± 0.3, with a range of 1.2–2.6. Mean TBR was 2.0 ± 0.5, with a range of 1.1–4.9. TBR was also highest in the abdominal aorta.

Calcified atherosclerotic lesions (Table 3) were detected at 6,456 sites in 42 (82.4%) of the 51 study patients. On average, 24.1 ± 25.4 (range, 1–125) CPs were found in each arterial segment with observable calcification, and the abdominal aorta showed the highest CP burden. Mean calcification thickness was 2.8 ± 1.3 mm (range, 1–8 mm).

Relationship Between ^{68}Ga-Pentixafor Uptake, CP Burden, and Cardiovascular Risk Factors

On a per-patient basis, 51 patients (100%) were PET-positive, 42 (82.4%) were CT-positive, 42 (82.4%) were PET-positive/CT-positive, and 9 (17.6%) were PET-positive/CT-negative.

On a per-segment basis, 330 (80.9%) of the 408 studied arterial segments were PET-positive, and 268 (65.7%) were CT-positive. There were on average 4.2 ± 3.3 (range, 1–16) sites of ^{68}Ga-pentixafor uptake in an affected segment, and 24.1 ± 25.4 (range, 1–125) calcified lesions.

On a per-lesion basis, 473 (33.5%) of the 1,411 arterial lesions with radiotracer accumulation showed concordant calcification. Only 7.3% of all arterial calcification sites showed increased ^{68}Ga-pentixafor uptake (Figs. 1 and 2). Consistent with these findings, there was a statistically significant correlation between the number of PET-positive arterial uptake sites and CP burden ($r = 0.67$, $P < 0.0001$), maximum plaque thickness ($r = 0.56$, $P < 0.0001$), and calcification score ($r = 0.69$, $P < 0.0001$), all describing different aspects of the extent of arterial calcification.

On average, study patients had 4 ± 2 (range, 1–7) cardiovascular risk factors. A significant correlation was found between the number of cardiovascular risk factors per patient and the number of CPs ($r = 0.46$, $P = 0.0007$), the number of PET-positive lesions ($r = 0.70$, $P < 0.0001$), and TBR ($r = 0.36$, $P = 0.009$) (Fig. 3). Single-variable regression analysis demonstrated significant correlations between the number of PET-positive arterial lesions and age at risk ($r = 0.60$, $P < 0.0001$), arterial hypertension ($r = 0.56$, $P < 0.0001$), hypercholesterolemia ($r = 0.47$, $P = 0.0005$), history of smoking ($r = 0.35$, $P = 0.01$), and prior vascular events ($r = 0.47$, $P = 0.0004$) (Supplemental Table 1; supplemental materials are available at http://jnm.snmjournals.org). Multiple regression analysis revealed age at risk ($r = 0.50$, $P = 0.0003$), arterial hypertension ($r = 0.52$, $P = 0.0001$), and history of smoking ($r = 0.36$, $P = 0.01$) to be independently associated with PET-positive arterial lesions (Supplemental Table 2).

Regarding the relationship of CP and cardiovascular risk factors, a significant correlation between CP burden and age at risk ($r = 0.51$, $P = 0.0001$), the presence of arterial hypertension ($r = 0.37$, $P = 0.008$), and prior vascular events ($r = 0.46$, $P = 0.0008$) was observed. Multiple regression analysis showed an independent association between CP burden and age at risk ($r = 0.49$, $P = 0.0003$) and prior vascular events ($r = 0.38$, $P = 0.008$).

Both the number of arterial uptake sites and the CP burden were significantly associated with current statin therapy ($P < 0.0001$ and $P = 0.0009$, respectively). TBR did not significantly differ between patients with (2.7 ± 0.8) and without (2.5 ± 0.8) ongoing statin treatment ($P = 0.23$).

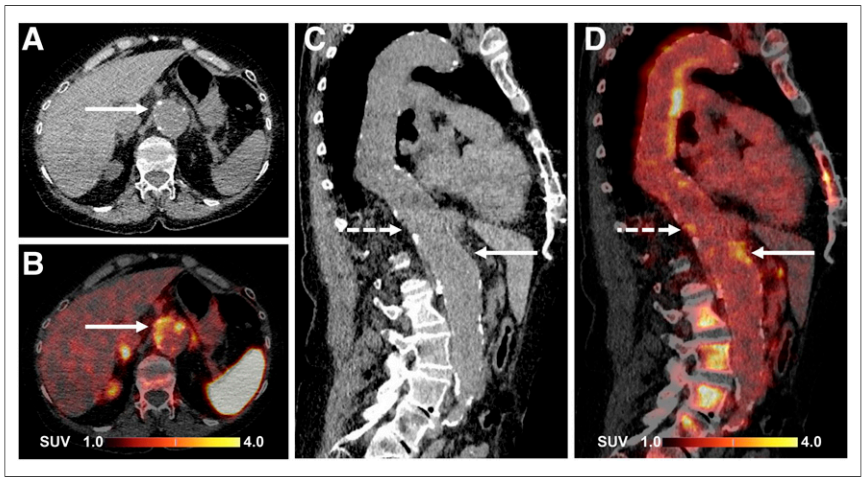

FIGURE 2. ^{68}Ga-pentixafor PET/CT images of abdominal aorta in 64-y-old woman. CT (A and C) and PET/CT (B and D) images in transaxial (A and B) and sagittal (C and D) views show ^{68}Ga-pentixafor uptake in partly calcified atherosclerotic lesion (solid arrows) in wall of atherosclerotic ectatic aorta. Sagittal views show additional foci of uptake in non-CP (dashed arrows).

DISCUSSION

To our knowledge, this was the first study of the prevalence, pattern, and clinical

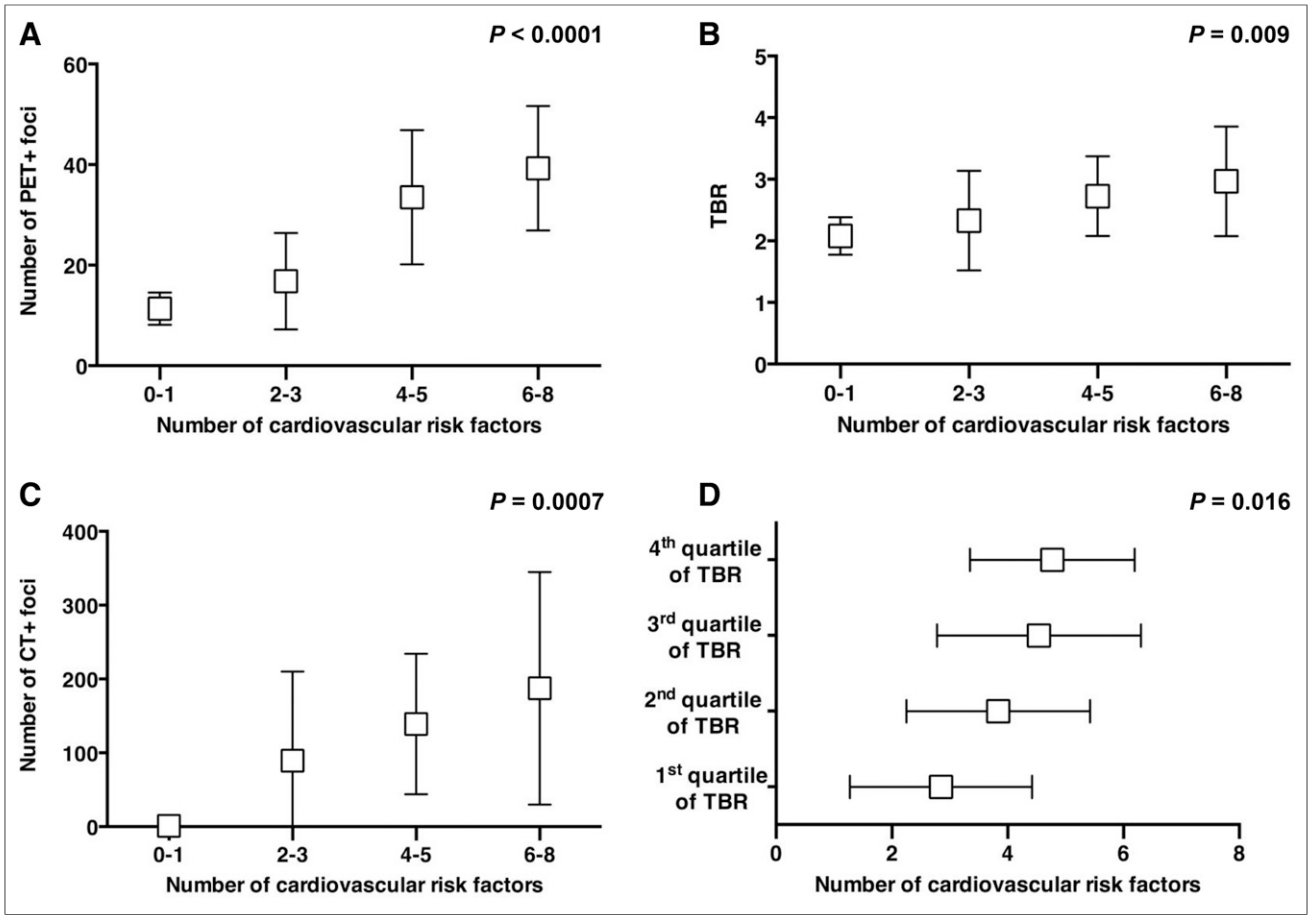

FIGURE 3. Correlation between imaging findings and number of cardiovascular risk factors. Number of CXCR4-positive lesions (A), TBR (B), and number of CPs (C) significantly increase as number of cardiovascular risk factors increases. TBR grouped by quartiles demonstrates high-risk profile in patients with high arterial CXCR4 expression (D).

correlates of large–arterial wall accumulation of ^{68}Ga-pentixafor in patients, and our results establish ^{68}Ga-pentixafor PET/CT for imaging of CXCR4 expression in the atherosclerotic vessel wall. This novel methodology may refine the characterization of atherosclerotic lesions and may serve as a platform for future clinical studies targeting CXCR4-positive cells in atherosclerosis.

The CXCR4/CXCL12 axis (Table 4) plays a pivotal role in atherosclerosis and arterial injury (*1,20*). In advanced plaque, the density of macrophages indicates the risk of an atherothrombotic event because macrophages release proteolytic enzymes degrading the fibrous cap and promote intralesional inflammation by secreting proinflammatory cytokines (*8*). Therefore, many commonly used tracers, including ^{18}F-FDG and ^{68}Ga-DOTATATE, are applied to visualize different aspects of macrophage density, the latter with limited success (*8,21*). Previous immunohistochemical analyses of CXCR4 expression in human atherosclerotic plaque revealed a progressive accumulation of CXCR4-positive cells during plaque evolution, and CXCR4-positive leukocytes have been detected in culprit lesions in acute coronary syndromes (*22*). Taken together, CXCR4 expression by leukocytes is associated with vulnerability of plaque. Indeed, vascular ^{68}Ga-pentixafor uptake showed a marked independent association with established risk factors such as at-risk age ($r = 0.50$, $P = 0.0003$), arterial hypertension ($r = 0.52$, $P = 0.0001$), and history of smoking ($r = 0.36$, $P = 0.01$). More important, both the number of CXCR4-positive lesions ($r = 0.70$, $P < 0.0001$) and the TBR ($r = 0.36$, $P = 0.009$) increased as the number of risk factors increased, suggesting a role for identifying risk-bearing atherosclerotic plaques.

Hyafil et al. have recently reported that CXCR4 expression is associated with CD68-positive macrophage-rich areas on immunohistochemistry of human carotid plaques (*15*). Additionally in that work, atherosclerotic plaques were induced by endothelial abrasion of large arteries in rabbits fed an atherogenic diet, leading to macrophage-rich plaques that were subsequently found to be CXCR4-positive (*15*). However, results from this nonphysiologic model of atherosclerotic plaque requiring both a considerable arterial injury and a special atherogenic diet may not be easily translated into the human clinical setting, in which atherogenic factors are much less pronounced, inflammation is not artificially induced and is less macrophage-dominated, and a variety of physiologic mechanisms are involved in the evolution of plaque. Indeed, other cell types involved in plaque evolution, including smooth muscle cell progenitors and endothelial progenitor cells, have also been found to express CXCR4 (*1*). Importantly, CXCR4 is also expressed by mature endothelial and smooth muscle cells in the arterial wall (*1*), indicating that other cell types may relevantly contribute to the in vivo CXCR4 signal. Arterial injury has been demonstrated to induce local smooth muscle cell CXCR4

TABLE 4
Involvement of CXCR4/CXCL12 Axis in Atherosclerosis and Arterial Injury

Cell type	Cell type–specific functions
Macrophages	Upregulation of CXCR4 by stimulation with oxidized low-density lipoprotein/statins/hypoxia/vascular injury
	→Chemotaxis and enhanced macropinocytosis, modulation of inflammatory phenotype
B and T cells	B-cell development and CXCR4-mediated chemotaxis
	→Pro-/antiatherogenic effects (phenotype-dependent)
Neutrophils	CXCR4-maintained homeostasis
	CXCR4-regulated neutrophil activation
Platelets	CXCR4-regulated amplification of platelet activation and platelet survival
Endothelial cells	Upregulation of CXCR4 by vascular endothelial growth factor/hypoxia/shear stress
	CXCL12/CXCR4 axis–mediated angiogenesis
	→Both detrimental effects (e.g., plaque neovascularization) and protective effects (e.g., preservation of endothelial barrier function, reendothelialization)
Vascular smooth muscle cells	CXCL12/CXCR4 axis–mediated proliferation and migration
	CXCR4 upregulation in injured arterial wall contributing to intimal hyperplasia
	→Both detrimental effects (e.g., neointimal hyperplasia) and protective effects (e.g., sustaining contractile phenotype, plaque stabilization by fibrous cap formation)

Modified from (*1,23,24*).

expression, contributing to intimal hyperplasia (*23*). This indicates that a portion of ^{68}Ga-pentixafor uptake could reflect mechanisms other than atherosclerosis, such as arterial injury in areas of turbulent flow. Finally, it has recently been shown that both CXCR4-positive endothelial cells and smooth muscle cells are atheroprotective in an apolipoprotein E–deficient mouse model, limiting atherosclerosis by maintaining arterial integrity and preserving endothelial barrier function (*24*). This finding underlines that CXCR4-positive cells have many different roles both in the atherosclerotic and in the nonatherosclerotic arterial wall (*1*). Although our results indicate a potential role of ^{68}Ga-pentixafor PET/CT as a tool not only for in vivo visualization of CXCR4-positive atherosclerotic lesions in the large arteries but also for identification of inflamed, rupture-prone plaques, the relative contribution of different pathophysiologic mechanisms and different cell types to the observed CXCR4 signal remains to be elucidated.

Of note, the ^{18}F-FDG signal in atherosclerotic lesions may be attenuated by use of statins. Likely because of the high cardiovascular risk profile, the number of arterial uptake sites and CP burden were higher in patients receiving statin treatment. However, the signal intensity (TBR) did not differ significantly between patients who were receiving ongoing statin treatment and those who were not ($P = 0.23$). These results are supported by recent data that found incubation with statins to have no significant impact on CXCR4 expression by macrophages (*15*), although other studies suggested some effect in certain monocyte subsets (*17*).

When the TBR of ^{68}Ga-pentixafor was analyzed, a good contrast between atherosclerotic lesions and the blood pool was found. The mean TBR of 2.0 ± 0.5 for CXCR4-positive lesions is comparable to the TBR of ^{18}F-sodium fluoride and even higher than the TBR of ^{18}F-FDG, facilitating the identification of atherosclerotic lesions (*10,16,25,26*). The distribution of ^{68}Ga-pentixafor throughout the major arteries was consistent with established atherosclerotic topography (*25–27*).

Although ^{68}Ga-pentixafor uptake was observed in all patients, CPs were less common (17.6% PET-positive/CT-negative patients). Interestingly, these patients were considerably younger than PET-positive/CT-positive patients (34.6 ± 8.8 vs 64.9 ± 11.8 y), suggesting that the presence of CXCR4-positive cells begins at an early age and precedes arterial calcification. Consistent with that observation, only 7.3% of all arterial calcification sites showed ^{68}Ga-pentixafor accumulation. CP is usually considered stable, late-stage atherosclerotic disease, underlining the possibility that CXCR4 imaging may identify earlier stages of plaque development and nonstable vulnerable plaque. Indeed, CXCR4-positive cells are involved in the initiation, progression, and rupture of atherosclerotic plaque (*1,7*). ^{18}F-FDG uptake representing a measure of macrophage density in plaque is likewise rarely seen in CP (*10,26*). Furthermore, ^{68}Ga-pentixafor uptake is clearly linked to the clinical cardiovascular risk profile, supporting a role for identifying risk-bearing plaque. The rate of colocalization between vascular ^{68}Ga-pentixafor accumulation and calcification was 33.5%, whereas for ^{18}F-FDG, coincident calcification was reported less frequently (*10,26*). These results indicate that CXCR4-targeted imaging may identify additional CXCR4-positive cells in the arterial wall besides intralesional macrophages, which represent the vascular target of ^{18}F-FDG PET. Indeed, CXCR4 is also expressed by a variety of progenitor and other cells in the arterial wall, including endothelial and vascular smooth muscle cells (*1*).

Some limitations of the present study should be acknowledged. First, the precise cell type contributing to the in vivo ^{68}Ga-pentixafor signal cannot be identified. However, previous ex vivo data evidenced upregulated CXCR4 expression by macrophages in atherosclerotic lesions (*15*). Second, the results of this study might not

be perfectly generalizable to other patient populations. However, factors that might affect physiologic processes in the vessel wall were carefully excluded. Third, scans were performed using a routine imaging protocol for ^{68}Ga-pentixafor imaging optimized for other indications. Dynamic or delayed data acquisition may provide additional information for the assessment of atherosclerotic plaques (*28*). ^{68}Ga-pentixafor exhibits a relatively high blood-pool signal. However, at least some part of that signal is caused by specific binding of ^{68}Ga-pentixafor on CXCR4-positive cells, questioning the potential impact of delayed imaging, which will rather support renal elimination of unbound tracer. In addition, the positron range is much higher for ^{68}Ga than for ^{18}F, potentially affecting the localization of the vessel wall signal and contributing to partial-volume effects. Given the facts that pentixafor is a specific marker of CXCR4-positive cell infiltration, that there are numerous preclinical studies linking plaque progression and CXCR4, and that established cardiovascular risk factors were strongly associated with tracer uptake in this study, we hypothesize that CXCR4-targeted PET imaging bears promise for stratifying the risk of impending atherothrombotic events.

CONCLUSION

On the basis of ex vivo findings of CXCR4 expression in atherosclerotic plaque, the present study demonstrated that ^{68}Ga-pentixafor PET/CT is suitable for noninvasive, highly specific clinical PET imaging of CXCR4 expression in the atherosclerotic wall of large arteries. ^{68}Ga-pentixafor uptake is significantly associated with CP burden and cardiovascular risk factors and may hold promise for identification of vulnerable plaque. This study provides a rationale to incorporate ^{68}Ga-pentixafor PET into further preclinical and clinical studies to obtain new insights into CXCR4 expression in atherosclerotic lesions and to evaluate whether it may be used to specifically monitor interventions targeting CXCR4.

DISCLOSURE

Saskia Kropf is the CEO of Scintomics. Dr. Hans-Juergen Wester is a shareholder of Scintomics. No other potential conflict of interest relevant to this article was reported.

REFERENCES

1. Döring Y, Pawig L, Weber C, Noels H. The CXCL12/CXCR4 chemokine ligand/receptor axis in cardiovascular disease. *Front Physiol.* 2014;5:212.
2. Ceradini DJ, Kulkarni AR, Callaghan MJ, et al. Progenitor cell trafficking is regulated by hypoxic gradients through HIF-1 induction of SDF-1. *Nat Med.* 2004;10:858–864.
3. Lim CS, Kiriakidis S, Sandison A, Paleolog EM, Davies AH. Hypoxia-inducible factor pathway and diseases of the vascular wall. *J Vasc Surg.* 2013;58:219–230.
4. Petit I, Jin D, Rafii S. The SDF-1–CXCR4 signaling pathway: a molecular hub modulating neo-angiogenesis. *Trends Immunol.* 2007;28:299–307.
5. Thackeray JT, Derlin T, Haghikia A, et al. Molecular imaging of the chemokine receptor CXCR4 after acute myocardial infarction. *JACC Cardiovasc Imaging.* 2015;8:1417–1426.
6. Lapa C, Reiter T, Werner RA, et al. [^{68}Ga]pentixafor-PET/CT for imaging of chemokine receptor 4 expression after myocardial infarction. *JACC Cardiovasc Imaging.* 2015;8:1466–1468.
7. Gupta SK, Pillarisetti K, Lysko PG. Modulation of CXCR4 expression and SDF-1 alpha functional activity during differentiation of human monocytes and macrophages. *J Leukoc Biol.* 1999;66:135–143.
8. Joseph P, Tawakol A. Imaging atherosclerosis with positron emission tomography. *Eur Heart J.* 2016;37:2974–2980.
9. Tarkin JM, Dweck MR, Evans NR, et al. Imaging atherosclerosis. *Circ Res.* 2016;118:750–769.
10. Derlin T, Tóth Z, Papp L, et al. Correlation of inflammation assessed by ^{18}F-FDG PET, active mineral deposition assessed by ^{18}F-fluoride PET, and vascular calcification in atherosclerotic plaque: a dual-tracer PET/CT study. *J Nucl Med.* 2011;52:1020–1027.
11. Gourni E, Demmer O, Schottelius M, et al. PET of CXCR4 expression by a ^{68}Ga-labeled highly specific targeted contrast agent. *J Nucl Med.* 2011;52:1803–1810.
12. Wester HJ, Keller U, Schottelius M, et al. Disclosing the CXCR4 expression in lymphoproliferative diseases by targeted molecular imaging. *Theranostics.* 2015;5:618–630.
13. Herrmann K, Lapa C, Wester HJ, et al. Biodistribution and radiation dosimetry for the chemokine receptor CXCR4-targeting probe ^{68}Ga-pentixafor. *J Nucl Med.* 2015;56:410–416.
14. Philipp-Abbrederis K, Herrmann K, Knop S, et al. In vivo molecular imaging of chemokine receptor CXCR4 expression in patients with advanced multiple myeloma. *EMBO Mol Med.* 2015;7:477–487.
15. Hyafil F, Pelisek J, Laitinen I, et al. Imaging the cytokine receptor CXCR4 in atherosclerotic plaques with the radiotracer ^{68}Ga-pentixafor for positron emission tomography. *J Nucl Med.* 2017;58:499–506.
16. Derlin T, Wisotzki C, Richter U, et al. In vivo imaging of mineral deposition in carotid plaque using ^{18}F-sodium fluoride PET/CT: correlation with atherogenic risk factors. *J Nucl Med.* 2011;52:362–368.
17. Jaipersad AS, Shantsila E, Blann A, Lip GY. The effect of statin therapy withdrawal on monocyte subsets. *Eur J Clin Invest.* 2013;43:1307–1313.
18. Demmer O, Gourni E, Schumacher U, et al. PET imaging of CXCR4 receptors in cancer by a new optimized ligand. *ChemMedChem.* 2011;6:1789–1791.
19. de Weert TT, Ouhlous M, Meijering E, et al. In vivo characterization and quantification of atherosclerotic carotid plaque components with multidetector computed tomography and histopathological correlation. *Arterioscler Thromb Vasc Biol.* 2006;26:2366–2372.
20. Weber C, Noels H. Atherosclerosis: current pathogenesis and therapeutic options. *Nat Med.* 2011;17:1410–1422.
21. Wan MYS, Endozo R, Michopoulou S, et al. PET/CT imaging of unstable carotid plaque with ^{68}Ga-labeled somatostatin receptor ligand. *J Nucl Med.* 2017;58:774–780.
22. Naruko T, Ueda M, Haze K, et al. Neutrophil infiltration of culprit lesions in acute coronary syndromes. *Circulation.* 2002;106:2894–2900.
23. Shi X, Guo LW, Seedial S, et al. Local CXCR4 upregulation in the injured arterial wall contributes to intimal hyperplasia. *Stem Cells.* 2016;34:2744–2757.
24. Döring Y, Noels H, van der Vorst EPC, et al. Vascular CXCR4 limits atherosclerosis by maintaining arterial integrity: evidence from mouse and human studies. *Circulation.* 2017;136:388–403.
25. Derlin T, Richter U, Bannas P, et al. Feasibility of ^{18}F-sodium fluoride PET/CT for imaging of atherosclerotic plaque. *J Nucl Med.* 2010;51:862–865.
26. Dunphy MPS, Freiman A, Larson SM, Strauss HW. Association of vascular ^{18}F-FDG uptake with vascular calcification. *J Nucl Med.* 2005;46:1278–1284.
27. Derlin T, Habermann CR, Lengyel Z, et al. Feasibility of ^{11}C-acetate PET/CT for imaging of fatty acid synthesis in the atherosclerotic vessel wall. *J Nucl Med.* 2011;52:1848–1854.
28. Blomberg BA, Thomassen A, Takx RA, et al. Delayed ^{18}F-fluorodeoxyglucose PET/CT imaging improves quantitation of atherosclerotic plaque inflammation: results from the CAMONA study. *J Nucl Cardiol.* 2014;21:588–597.